Article

Broad Range Tuning of InAs Quantum Dot Emission for Nanophotonic Devices in the Telecommunication Bands

Bianca Scaparra,* Elise Sirotti, Akhil Ajay, Björn Jonas, Beatrice Costa, Hubert Riedl, Pavel Avdienko, Ian D. Sharp, Gregor Koblmüller, Eugenio Zallo, Jonathan J. Finley, and Kai Müller

Read Online

ACCESS | Metrics & More | Article Recommendations

ABSTRACT: InAs semiconductor quantum dots (QDs) emitting in the near-infrared are promising platforms for on-demand single-photon sources and spin-photon interfaces. However, the realization of quantum-photonic nanodevices emitting in the telecom windows with similar performance remains an open challenge. In particular, nanophotonic devices incorporating quantum light emitting diodes in the telecom C-band based on GaAs substrates are still lacking due to the relaxation of the lattice constant along the InGaAs graded layer which makes the implementation of electrically contacted devices challenging. Here, we report an optimized heterostructure design for QDs emitting in the telecom O- and C-bands grown by means of molecular beam epitaxy. The InAs QDs are embedded in mostly relaxed InGaAs matrices with fixed indium content grown on top of compositionally graded InGaAs buffers. Reciprocal space maps of the indium profiles and optical absorption spectra are used to optimize $In_{0.22}Ga_{0.78}As$ and $In_{0.30}Ga_{0.70}As$ matrices, accounting for the chosen indium grading profile. This approach results in a tunable QD photoluminescence (PL) emission from 1200 up to 1600 nm. Power and polarization dependent micro-PL measurements performed at 4 K reveal exciton-biexciton complexes from quantum dots emitting in the telecom O- and C-bands. The presented study establishes a flexible platform that can be an essential component for advanced photonic devices based on InAs/GaAs that serve as building blocks for future quantum networks.

KEYWORDS: quantum dots, telecommunication spectral range, molecular beam epitaxy, compositionally graded layers, X-ray diffraction
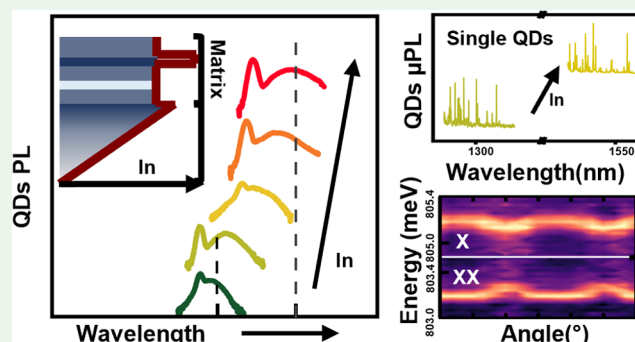
■ INTRODUCTION

Photonic quantum technologies require sources that emit photons at a fast rate and with a high degree of indistinguishability. Semiconductor quantum dots (QDs) emitting at 950 or 785 nm have been demonstrated to be very promising systems to meet these demands.[1−5] Indeed, the implementation of resonators,[6−8] combined with the ability to tune the QDs emission wavelengths via the Stark effect and to electrically control the surrounding electronic environment,[9] make InAs QDs excellent building blocks for quantum communication protocols. In this regard, the possibility to achieve equal performance at telecom wavelengths would be especially appealing due to the pre-existing fiber infrastructure and low propagation losses.[10] Emission in the telecom C-band is obtained by means of InAs QDs based heterostructures grown on InP substrates,[11−13] whereas compositionally graded InGaAs layers are needed for the case of InAs QDs on GaAs substrates to reduce their lattice mismatch.[14−16] While the InAs/InP system allows for direct implementation of cavities by using Bragg gratings or photonic crystals,[17−20] an optimized nonlinear grading profile was suggested for the second

heterostructure.[21,22] However, despite the thinner graded layer due to the nonlinear grading profile, the relaxed portion of the graded layer was included in the fabricated resonator, thus limiting the further implementation of electrical contacts or more elaborate postprocessing. GaAs substrates offer the possibility to grow lattice-matched high refractive index contrast distributed Bragg reflectors and are less brittle than InP substrates. Additionally, metamorphic laser heterostructures emitting in the telecom bands grown on GaAs substrates have proven to be compatible with the implementation in the matrices grown on top of the graded layers of gate-tunable devices and sacrificial layers.[23−26] A similar approach has also been effective in realizing emission sources in the telecom C-band,[27] however a tunable indium grading design resulting in
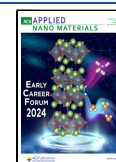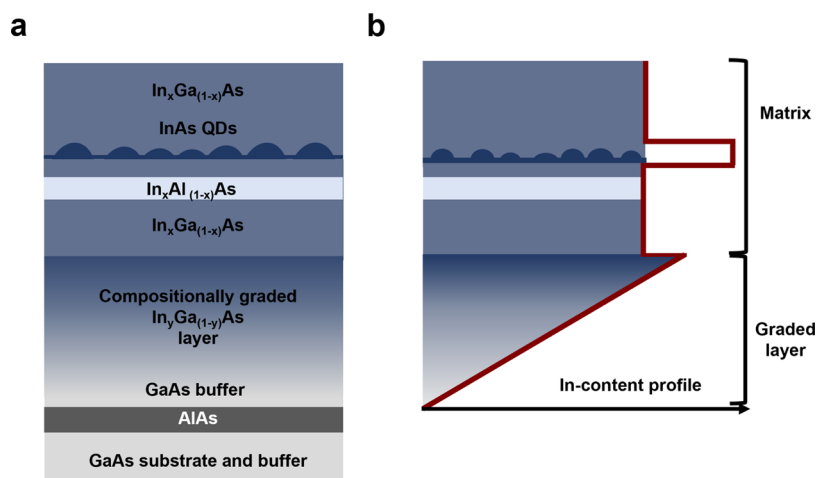
Figure 1. (a) Schematic of the investigated sample structure: the InAs QDs and InAlAs layers are embedded in an InGaAs-matrix with fixed indium content grown on top of a compositionally graded InGaAs layer. The graded layer is grown on top of a AlAs and GaAs buffer layers grown on a (001) GaAs substrate. (b) Schematic of the indium profile across the grown heterostructures starting from the compositionally graded InGaAs layer.

high-quality QD emission from telecom O- to the C-bands is still coveted.

In this paper, we develop a grading design in which the InAs QD layer is embedded in an InGaAs matrix with fixed indium content that is carefully chosen depending on the maximum relaxation reached in the underlying graded layer. Using reciprocal space maps and optical absorption measurements, we determine the indium profiles that best match the used indium grading rate. In particular, we identify a favorable indium concentration step-back value between the matrix and graded layer as a function of the grading rate of the latter. The matrix acts as an independent substrate with chosen lattice constant and the dislocations are mostly confined to the relaxed part of the graded layer. By embedding a single QD layer in the matrix, we demonstrate the tunability of the lattice constant of the final substrate resulting in a QD emission in both the telecom O- and C-bands. Power and polarization dependent photoluminescence measurements reveal bright and sharp lines with the typical exciton-biexciton behavior. This study highlights the potential of the presented design toward the realization of electrically contacted nanodevices for ideal single-photon sources in the telecom O- and C-bands.

■ MATERIALS AND METHODS

The studied samples were grown with a solid source Veeco Gen II molecular beam epitaxy (MBE) system on undoped GaAs(001) substrates. The growth was monitored by reflection high energy electron diffraction and the native oxide desorption from the substrate was used to calibrate the surface temperature. The layer profile is presented in Figure 1a. First, a 200 nm-thick GaAs buffer layer was grown, followed by a 100 nm-thick AlAs layer to provide higher contrast in scanning electron microscopy measurements. Both layers were grown at 610 °C. Subsequently, 30 nm of GaAs and a compositionally graded $In_xGa_{1-x}As$ layer were grown at 470 °C with an arsenic beam equivalent pressure of 1.6×10^{-5} mbar. The group-III elemental fluxes (gallium, indium, aluminum) were calibrated in equivalent growth rate units of Å/s. During the growth of the graded $In_xGa_{1-x}As$ layer, the gallium growth rate was kept constant at 1 Å/s, while the indium cell temperature was increased with a nominal rate of 0.02 °C/s. The indium growth rate was then increased from 0.05 Å/s to either 0.58 Å/s or 0.75 Å/s depending on the desired final lattice constant of the designed graded layer. The graded layer was then followed by an InGaAs matrix. The matrix presents a fixed

indium content and was grown with a lower indium cell temperature, as depicted by the step-back in the indium profile shown in Figure 1b. The indium contents of the InGaAs matrices were varied from 19 to 36% depending on the maximum indium content of the underlying compositionally graded layer. During the growth of the InGaAs matrix, the substrate temperature was increased to 500 °C and the arsenic beam equivalent pressure was reduced to 1.1×10^{-5} mbar. After a 150 nm-thick InGaAs layer, a 100 nm-thick InAlAs layer was grown to prevent further propagation of dislocations into the matrix.[28,29] The InAs QD layer, consisting of 2.2 monolayers, was grown at 470 °C and was embedded in the middle of a 300 nm-thick InGaAs layer. To achieve a QD density gradient, the substrate rotation was stopped halfway through the growth of the QD layer.

Structural characterization was performed via high-resolution X-ray diffraction measurements acquired with a Rigaku SmartLab system equipped with a copper anode. The $Cu_{K\alpha1}$ emission line ($\lambda = 1.54059$ Å) was filtered in the incident beam path with a Ge(220)x2 monochromator for high-resolution measurements. Reciprocal space maps (RSMs) around the asymmetric GaAs (422) reflection were used to analyze the crystalline properties of the grown heterostructures. The absorption coefficients of the InGaAs matrices grown on top of the graded layer were measured with a custom-made photothermal deflection spectroscopy (PDS) system. The sample was placed into a cuvette filled with perfluorohexane and illuminated at normal incidence with light whose wavelength was tuned across the desired range with a monochromator placed after a Halogen lamp. The modulation frequency of the incident light was set at 9 Hz. The absorption was probed with a red laser diode directed parallel to the surface of the sample. A two-dimensional (2D) detector connected to a lock-in amplifier was used to track the deflected probe laser beam. The PDS signal was then converted to an absorption coefficient with the layer thickness determined from scanning electron microscopy measurements. Temperature-dependent PL spectroscopy from ensembles of InAs QDs was performed under continuous wave nonresonant excitation at 660 nm by using a helium flow cryostat operating in the 4−300 K temperature range. Micro-PL measurements were carried out at 4 K using a confocal microscopy setup based on continuous wave excitation at 780 nm and an apochromatic objective with a numerical aperture of 0.81. The detected signal was analyzed using a spectrometer with a focal distance of 750 mm equipped with an InGaAs linear array detector, providing a resolution of 51 μeV at 1550 nm and of 71 μeV at 1310 nm. Polarization-resolved measurements were carried out by detecting the emitted signal as a function of the angle of a half-waveplate placed in front of a linear polarizer in the detection path.

■ RESULTS AND DISCUSSION

To realize the heterostructure presented in Figure 1a, the compositionally graded In$_x$Ga$_{1-x}$As layer first had to be optimized in order to obtain the desired final lattice constant. Depending on its final value, the indium content of the matrix, or final substrate, was then selected.

Figure 2a shows RSMs along the asymmetric (422) GaAs reflection of two different heterostructures, each consisting of a
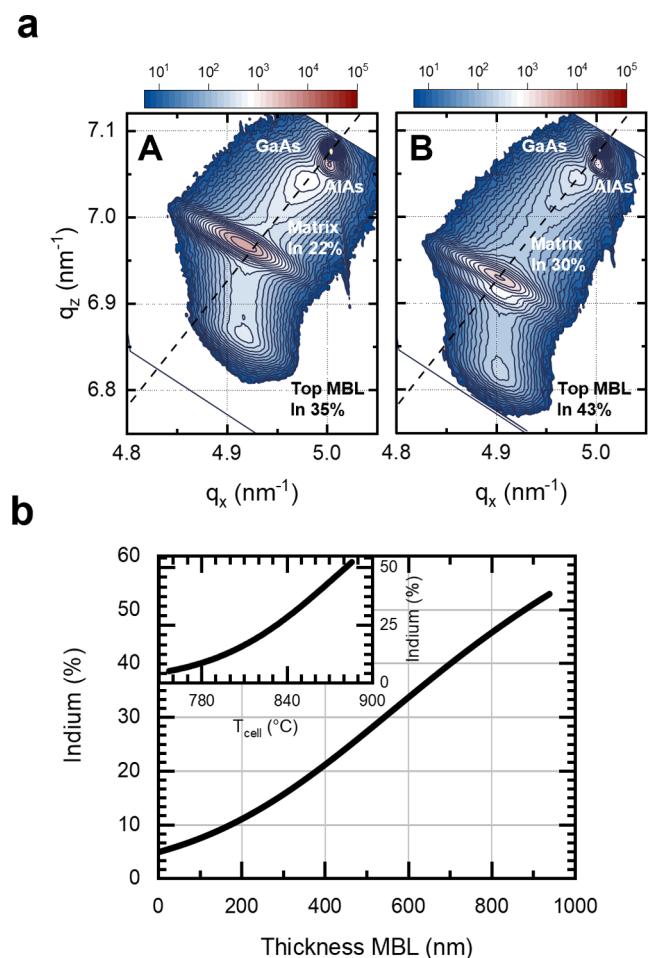

Figure 2. (a) RSMs along the asymmetric (422) GaAs reflection from heterostructures with different maximum indium contents in the compositionally graded layers grown beneath InGaAs matrices with indium contents of 22% (sample **A**) and 30% (sample **B**). (b) Indium content as a function of the thickness of the InGaAs graded layer at a fixed gallium rate. The inset shows the dependence of the indium content as a function of the indium cell temperature T_{cell} at a fixed gallium rate.

graded buffer layer and an InGaAs matrix grown on top. The heterostructure **A** was grown with a maximum indium growth rate in the graded layer of 0.58 Å/s, while in sample **B** the maximum growth rate was 0.75 Å/s. The peak at larger coordinates arises from the GaAs substrate, while the diffraction signal spanning from the GaAs peak to the lowest q_x and q_z values originates from the compositionally graded layer. Intensity maxima with coordinates close to the GaAs substrate correspond to areas of the graded layer with lower indium content, whereas peaks located further away indicate regions with higher indium content. The dashed line illustrates the relaxation line, which corresponds to the direction in

reciprocal space of a fully relaxed epitaxial layer. The signal arising from the layers with low indium content follows the relaxation line, revealing relaxed layers where the majority of the dislocations are confined.[30] Meanwhile, the part of the graded layers with higher indium content grows pseudomorphically to such relaxed layers, showing a constant q_x value and indicating the indium content at which the compositionally graded layer starts to show residual strain.[31,32] The derived maximum indium contents in the graded layers are 35% (**A**) and 43% (**B**), determined following an approach similar to ref[30]. The signal spreading in diagonal directions stems from the mostly relaxed matrices with indium contents of 22 and 30%, respectively. Both exhibit some mosaicity. As desired, the peaks arising from the layers in the matrices have the same q_x values as those of the relaxed part of the graded layer at higher indium contents. Hence, the two layers show similar in-plane lattice constants and thus, the probability of dislocation propagation into the matrix is reduced.[33] Due to the chosen grading rate and growth temperature of the InGaAs graded layers, we expect that near-equilibrium strain relaxation was reached.[30]

It has been shown that the residual strain in the uppermost part of a linearly graded layer is independent of both its thickness and the maximum indium concentration.[31,32,34,35] Thus, the indium step-back in the matrix, needed to compensate for the residual strain of a graded layer, depends on the chosen grading rate.[34] Although the indium profile set by the temperature ramping rate of the indium cell is not strictly linear along the graded layer as shown in Figure 2b, we found that an indium step-back close to ∼13% leads to a mostly relaxed matrix for both sample **A** and **B**. This is consistent with previous literature, where for a linear grading rate of ∼30 In%/μm, the indium step-back required to compensate for the residual strain was determined to be ∼8.3%.[31,32,34] Consequently, the higher average grading rate used in this study (∼49 In%/μm) would result in a larger degree of residual strain,[34] thus leading to a larger amount of indium step-back. Figure 2b shows the final indium profile with some nonlinearities across the graded layer. This is the result of the indium content dependence as a function of the cell temperature (see the inset at fixed gallium rate of 1 Å/s). Also for the grading profile shown in Figure 2b, similar amounts of indium step-back are found for both samples **A** and **B** (see Figure 2a) regardless of the maximum composition of the graded layer, as predicted by the models presented in refs 34,35. Therefore, to minimize a further relaxation of the graded layer, the indium content selected for the matrix was closely matched to the value determined based on the chosen grading profile. It is worth mentioning that a similar study could be carried out for the case of different grading profiles, as in the case of a step-graded growth of the compositionally graded layer, once the incomplete relaxation is taken into account for the further growth of the matrix.[36]

Figure 3a shows optical absorption spectra measured via PDS[37] from samples with matrices grown with different indium contents. Each curve is labeled with the indium content of the matrix determined from asymmetric RSMs. All spectra exhibit similar absorption around 1.42 eV (dashed line), which is attributed to the absorption at the bandgap of the GaAs substrate. In addition, absorption onsets around 1.1 eV (0.9 eV) are observed for samples in which InGaAs matrices are grown atop the compositionally graded layers with maximum indium contents of 35% (43%). The linear regressions of the
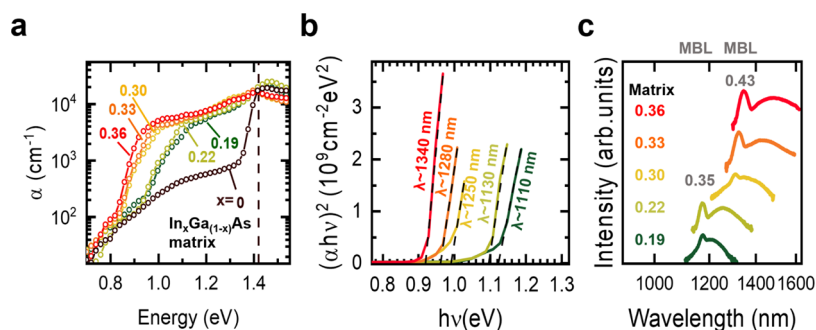
Figure 3. (a) Absorption coefficients α recorded by PDS from samples with indium content in the matrices ranging between 19 and 36% (maximum indium content in the graded layer of 35 and 43%). (b) Tauc plot of $(\alpha h\nu)^2$ plotted versus the absorption energy $h\nu$. The intersections of the dashed lines with the energy axis indicate the direct absorption edges of the InGaAs matrices. The determined bandgap is labeled as λ. (c) Ensemble PL spectra recorded at 10 K from QDs embedded in heterostructures with different indium content in the matrices grown on graded layers having 35 and 43% maximum indium content.
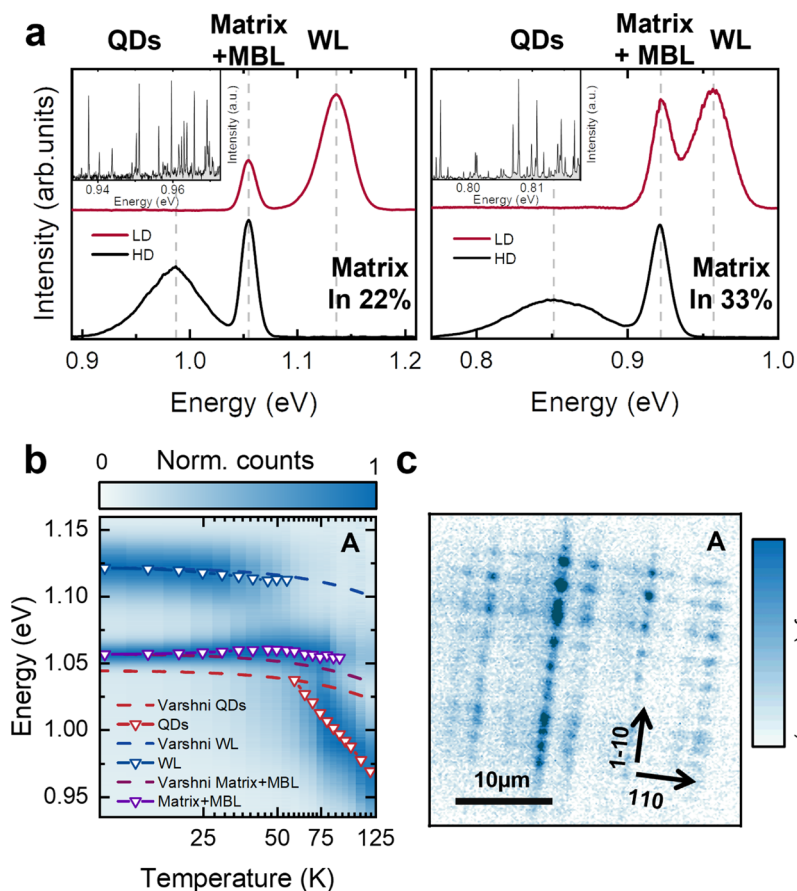

Figure 4. (a) Representative PL spectra acquired in regions with low (LD, red) and high (HD, black) QD density. (Insets) Microphotoluminescence spectra for each of the presented samples measured at 4 K, showing single emission lines from a set of QDs. (b) Ensemble PL spectra as a function of the lattice temperature from heterostructure **A**. The peak positions of QD, matrix, and WL (triangles) are plotted together with the bandgap shrinkage of bulk InAs (dashed lines) shifted with repect to the QDs, matrix, and WL emissions at 10 K. (c) Micro-PL map of sample **A** recorded at 4 K, showing QDs emitting in the spectral range of 1250−1350 nm.

Tauc plots shown in Figure 3b allow to estimate the optical bandgaps of the InGaAs matrices. The color scale follows the indium contents labeled in Figure 3a. Prior to performing the linear regression, each spectrum was divided by the spectrum recorded from the bare GaAs substrate, as the optical absorption of the substrate is stronger than the one from the matrices. The intersections of the linear regions of the $(\alpha h\nu)^2$ vs $h\nu$ plots with the energy axis indicate the optical bandgaps,[38] as labeled in Figure 3b with λ. The optical bandgaps obtained

by linear regression correspond to indium contents similar to the ones measured via RSMs.

To prove whether the presented sample designs lead to a QD emission in the telecom bands, ensemble PL measurements were taken at low temperature by exciting at 780 nm. As shown in Figure 3c, the variation of the lattice mismatch due to different indium contents in the matrix leads to a shift of the QD PL emission to the second and even further to the third telecom windows. Two peaks can be distinguished in each
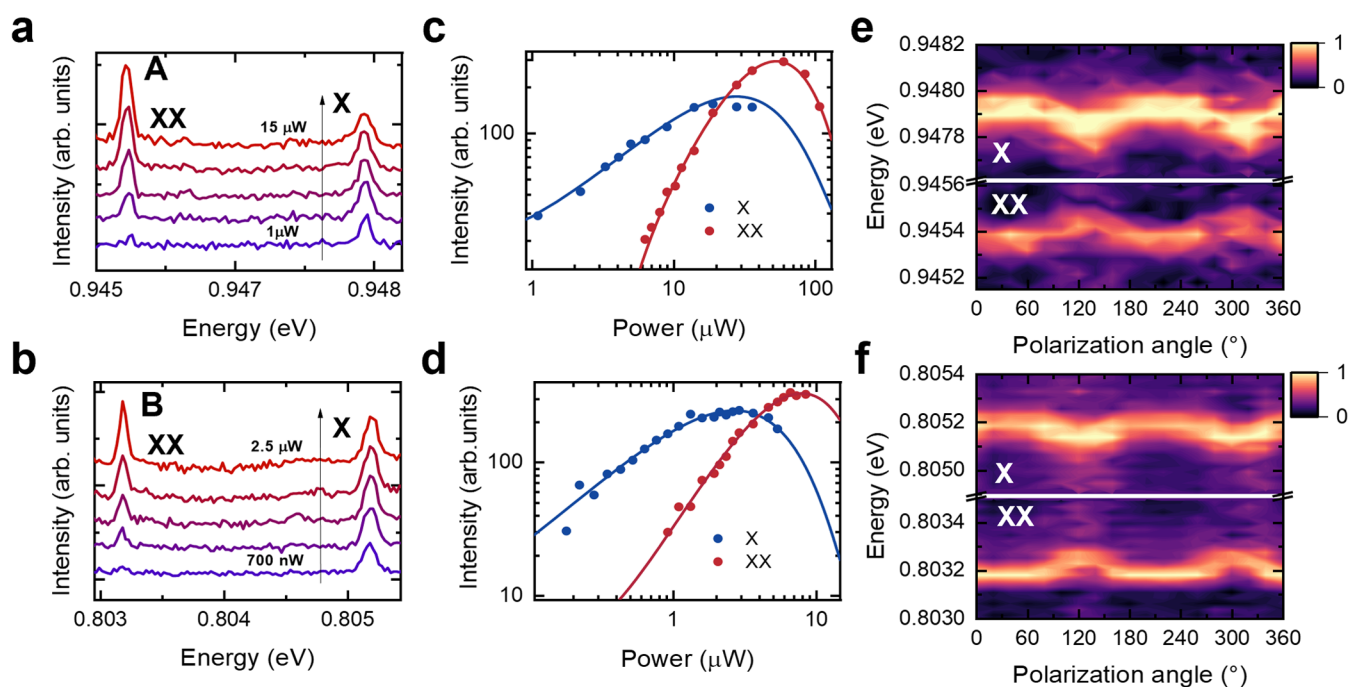
Figure 5. (a, b) Micro-PL spectra of QDs emitting in the O- and C-band measured from samples **A** and **B**. The spectra were recorded at 4 K under nonresonant excitation at different excitation powers. (c, d) Integrated intensity of the emission lines shown in (a, b) respectively. The data were fitted with Poissonian distributions $I(P) = a \cdot (P^n/n!) \cdot e^{b \cdot P} + I_0$ as a function of the power, yielding the probability that the QD is occupied with $n = 1$ (blue) or $n = 2$ (red) excitons complexes. (e, f) Polarization dependence of the emission energies of the X and XX emission lines from QDs emitting in the telecom O- and C-bands, respectively.

spectrum: the one at shorter wavelengths is attributed to charges recombining in the graded layer and the matrix, while the emission at longer wavelengths is attributed to the QDs. Samples with matrices with indium contents between 19 and 22% (maximum graded layer indium content of 35%) lead to a QD emission that can be tuned across the O-band. When the indium in the matrices ranges between 30 and 36% (maximum graded layer indium content of 43%) the QD emission shifts up to the telecom C-band. It is important to note that samples with indium step-back much lower than 13%, e.g., the one with a indium content of 36%, result in a matrix that is compressively strained with respect to the matrix. Since this could lead to further relaxation in the graded layer,[34] such sample was not considered for further optical measurements.

Figure 4a shows ensemble spectra obtained under above-bandgap excitation at a power of 600 μW from samples with matrix indium contents of 22 and 33%, recorded in regions of the wafer with different QD densities. If the QD density is low enough (LD, red), the injected charges mostly recombine in the wetting layer (WL), leading to the appearance of the peaks at higher energies. Meanwhile, in regions where the QD density increases (HD, black), the signal from charges recombining in the WL is quenched and the QD peak appears at lower energies in both graphs. The peaks centered around 1.05 and 0.92 eV are due to charges recombining in the matrix and in the uppermost regions of the graded layer (see Figure 1b). The insets show bright and sharp lines in the telecom O and C-bands attributed to PL emission of a few QDs excited at a wavelength of 780 nm. The respective full width at half-maximum (fwhm) values of the emissions is 89 ± 15 μeV (matrix 22%) and 90 ± 22 μeV (matrix 33%), which are limited by the spectrometer resolution.

The assignment of the peaks presented in Figure 4a is further confirmed by the temperature dependent PL recorded from sample **A**, as shown in Figure 4b. The spectra were recorded in a similar region where the spectrum LD was measured and were normalized with respect to the peak maxima. The measurements were performed under above-bandgap excitation with a power of 300 μW. Each spectrum was fitted with Gaussian profiles and the corresponding center peak positions are shown for each temperature. The fitted spectral positions are overlaid with the InAs Varshni relation (dashed lines), which indicates the dependence of the bandgap of bulk InAs on the lattice temperature.[39,40] At 10 K the emissions attributed to the WL (blue triangles) and the matrix (purple triangles) are visible. When the temperature reaches 60 K, another peak at lower energies appears, which is attributed to the QD emission (red triangles), while the one that stems from the WL quenches. This marks the temperature at which the charge transfer mechanism from the WL states to the QD ones becomes favorable.[30,41] The QD peaks show the typical steeper spectral redshift when compared to the Varshni relation (dashed lines). This can be attributed to charge redistribution into QDs with lower energy ground states.[30,42] In contrast, the WL peak follows the behavior given by the Varshni relation until it quenches at 60 K in favor of the QD emission. Meanwhile, the signal arising from the matrix and graded layer persists up to 110 K before vanishing. Figure 4c shows a 25 × 25 μm^2 micro-PL spatial map from sample **A** recorded at 4 K. The existence of periodic modulations on the surface, and thus in the QD formation, is a hallmark of the underlying dislocation network due to the plastic relaxation in the graded layer.[14,27,30] The image shows an area of the sample in which the QD density is on the order of ~10^9 cm^{-2}. The pattern resulting from optically active QDs resembles the one

from the cross-hatched surfaces along the [110]-[1$\bar{1}$0] directions typical for metamorphic surfaces.[43−46] As implied by the figure, the QD nucleation tends to follow the surface undulations along the [1$\bar{1}$0] direction,[14,30,47] which is the result of the indium composition modulation[27] and thus, strain fluctuation in the matrix. This confirms the non uniform strain distribution across the InGaAs matrix.

Micro-PL experiments on samples **A** and **B** were carried out at 4 K in order to identify excitonic complexes in the second and third telecom windows. Figure 5a,b show the power dependent PL of exciton-biexciton complexes. The marked emission lines can be identified as excitons (X) and biexcitons (XX) separated by binding energies of 2.5 and 2 meV in the O and C-telecom bands, respectively, similar to the values reported in literature.[16,30,42] This assignment is further corroborated via power dependent and polarization resolved measurements. In Figure 5c,d the integrated intensities of the transition are presented as a function of the excitation power. The data follow Poissonian distributions, where an average number of generated excitons equal to one (blue dots) correspond to X transitions. Meanwhile, the data corresponding to an average number of two generated excitons (red dots) correspond to XX transitions.[48] At low powers, the X transitions show a linear dependence on the excitation power, while the XX transitions only appear at higher powers and exhibit a quadratic behavior. For powers greater than the ones at which the X emission saturates, the XX emission prevails. The fwhm's from X and XX of Figure 5a, measured in the X saturation regime, are 123 and 90 μeV, respectively, while values of 107 and 54 μeV are measured from the respective lines in Figure 5b. These values are lower than the average ones reported for QDs grown directly on MBE-grown metamorphic buffer layers (around 200−300 μeV for emissions in the telecom O- and C-bands).[16] We attribute the reported line widths to the optimized growth condition of the graded buffer[30] and to the careful choice of the indium content in the matrix to account for the incomplete relaxation of the graded layer beneath. Smaller line widths have been reported for QDs grown directly on InGaAs graded layers grown via metal organic vapor phase epitaxy[14] that allows for the implementation of a linear grading profile along the graded layer. Linear profiles can be envisioned in MBE grown samples by adapting the temperature ramping rate of the indium cell during the growth of the graded layer.[35] Polarization-dependent normalized PL measurements shown in Figure 5e,f support the assigned excitonic behaviors. The measurements were carried out in the saturation regime of the X transitions. The counter-oscillating behavior of the spectral oscillations that present the same amplitude is typical of a XX-X cascade.[49] From fits to these data, we extract fine structure splittings of 60 ± 6 and 55 ± 6 μeV for the QDs shown in Figure 5e,f, respectively. The fine structure splittings could be reduced by further optimizing the growth parameters for the QD layer[50] or by piezoelectric strain tuning.[51] Furthermore, growing the QDs via droplet epitaxy has been proved to consistently lead to smaller fine structure splittings values.[52] These results confirm the effectiveness of the studied indium profiles along the heterostructure in tuning the QD emission over a large spectral region. They also demonstrate the successful design of the virtual substrates, which can be overgrown with substrates with tailored lattice constants.

■ CONCLUSIONS AND OUTLOOK

In this paper, we investigated indium concentration profiles within metamorphic substrates tailored to achieve a QD emission in the telecom O- and C-bands. The graded layers were overgrown with InGaAs matrices and act as virtual substrates. By means of reciprocal space maps and optical absorption measurements, the indium step-back value between the compositionally graded layer and matrix was optimized to guarantee a good relaxation degree of the latter for the adopted indium grading profile. Low temperature PL spectra showed the tunability of the QD emission as a function of the indium content in the matrix. The reported excitonic complexes in the telecom O- and C-bands proved the effectiveness of the heterostructure design also showing narrow line widths of the excitonic transitions. One major advantage of the presented heterostructures is the possibility to grow InAs QDs on optimized substrates with tailored lattice constants. The control of the mismatch between the QDs and the final substrate enables the tuning of their emission from 1200 up to 1600 nm. Another advantage lies in the confinement of dislocations caused by the plastic relaxation of the lattice constant, primarily within the graded layer grown beneath the final substrate. The possibility of growing barriers or superlattices in the InGaAs matrix beneath the QDs helps prevent further propagation of the dislocations across the matrix. We anticipate this study to be the first step toward developing quantum light emitting diodes at 1550 nm that are also compatible with integrated photonics on silicon based on GaAs/InAs material systems.

■ AUTHOR INFORMATION

Corresponding Author

Bianca Scaparra − *Walter Schottky Institut, Technical University of Munich, Garching 85748, Germany; TUM School of School of Computation, Information and Technology, Department of Electrical Engineering, Technical University of Munich, Garching 85748, Germany; Munich Center for Quantum Science and Technology (MCQST), Munich 80799, Germany;* ⊙ orcid.org/0009-0009-7420-5934; Email: bianca.scaparra@wsi.tum.de

Authors

Elise Sirotti − *TUM School of School of Natural Sciences, Department of Physics, Technical University of Munich, Garching 85748, Germany; Walter Schottky Institut, Technical University of Munich, Garching 85748, Germany;* ⊙ orcid.org/0009-0001-5212-0990

Akhil Ajay − *TUM School of School of Natural Sciences, Department of Physics, Technical University of Munich, Garching 85748, Germany; Walter Schottky Institut, Technical University of Munich, Garching 85748, Germany; Munich Center for Quantum Science and Technology (MCQST), Munich 80799, Germany;* ⊙ orcid.org/0000-0001-5738-5093

Björn Jonas − *Walter Schottky Institut, Technical University of Munich, Garching 85748, Germany; TUM School of School of Computation, Information and Technology, Department of Electrical Engineering, Technical University of Munich, Garching 85748, Germany; Munich Center for Quantum Science and Technology (MCQST), Munich 80799, Germany*

Beatrice Costa − *Walter Schottky Institut, Technical University of Munich, Garching 85748, Germany; TUM*

School of School of Computation, Information and Technology, Department of Electrical Engineering, Technical University of Munich, Garching 85748, Germany; Munich Center for Quantum Science and Technology (MCQST), Munich 80799, Germany

Hubert Riedl − *Walter Schottky Institut, Technical University of Munich, Garching 85748, Germany; TUM School of School of Natural Sciences, Department of Physics, Technical University of Munich, Garching 85748, Germany; Munich Center for Quantum Science and Technology (MCQST), Munich 80799, Germany*

Pavel Avdienko − *Walter Schottky Institut, Technical University of Munich, Garching 85748, Germany; TUM School of School of Natural Sciences, Department of Physics, Technical University of Munich, Garching 85748, Germany; Munich Center for Quantum Science and Technology (MCQST), Munich 80799, Germany*

Ian D. Sharp − *Walter Schottky Institut, Technical University of Munich, Garching 85748, Germany; TUM School of School of Natural Sciences, Department of Physics, Technical University of Munich, Garching 85748, Germany;* orcid.org/0000-0001-5238-7487

Gregor Koblmüller − *Walter Schottky Institut, Technical University of Munich, Garching 85748, Germany; TUM School of School of Natural Sciences, Department of Physics, Technical University of Munich, Garching 85748, Germany; Munich Center for Quantum Science and Technology (MCQST), Munich 80799, Germany;* orcid.org/0000-0002-7228-0158

Eugenio Zallo − *Walter Schottky Institut, Technical University of Munich, Garching 85748, Germany; TUM School of School of Natural Sciences, Department of Physics, Technical University of Munich, Garching 85748, Germany; Munich Center for Quantum Science and Technology (MCQST), Munich 80799, Germany;* orcid.org/0000-0003-1796-9777

Jonathan J. Finley − *Walter Schottky Institut, Technical University of Munich, Garching 85748, Germany; TUM School of School of Natural Sciences, Department of Physics, Technical University of Munich, Garching 85748, Germany; Munich Center for Quantum Science and Technology (MCQST), Munich 80799, Germany*

Kai Müller − *Walter Schottky Institut, Technical University of Munich, Garching 85748, Germany; TUM School of School of Computation, Information and Technology, Department of Electrical Engineering, Technical University of Munich, Garching 85748, Germany; Munich Center for Quantum Science and Technology (MCQST), Munich 80799, Germany*

Complete contact information is available at:
https://pubs.acs.org/10.1021/acsanm.4c04810

Notes

The authors declare no competing financial interest.

■ REFERENCES

(1) Senellart, P.; Solomon, G.; White, A. High-performance semiconductor quantum-dot single-photon sources. *Nat. Nanotechnol.* **2017**, *12*, 1026−1039.

(2) Hanschke, L.; Fischer, K.; Appel, S.; Lukin, D.; Wierzbowski, J.; Sun, S.; Trivedi, R.; Vučković, J.; Finley, J. J.; Müller, K. Quantum dot single-photon sources with ultra-low multi-photon probability. *npj Quantum Inf.* **2018**, *4*, No. 43.

(3) Sbresny, F.; Hanschke, L.; Schöll, E.; Rauhaus, W.; Scaparra, B.; Boos, K.; Casalengua, E. Z.; Riedl, H.; del Valle, E.; Finley, J. J.; Jöns, K. D.; Müller, K. Stimulated Generation of Indistinguishable Single Photons from a Quantum Ladder System. *Phys. Rev. Lett.* **2022**, *128*, No. 093603.

(4) da Silva, S. F. C.; Undeutsch, G.; Lehner, B.; Manna, S.; Krieger, T. M.; Reindl, M.; Schimpf, C.; Trotta, R.; Rastelli, A. GaAs quantum dots grown by droplet etching epitaxy as quantum light sources. *Appl. Phys. Lett.* **2021**, *119*, No. 120502.

(5) Schöll, E.; Hanschke, L.; Schweickert, L.; Zeuner, K. D.; Reindl, M.; da Silva, S. F. C.; Lettner, T.; Trotta, R.; Finley, J. J.; Müller, K.; Rastelli, A.; Zwiller, V.; Jöns, K. D. Resonance Fluorescence of GaAs Quantum Dots with Near-Unity Photon Indistinguishability. *Nano Lett.* **2019**, *19*, 2404−2410.

(6) Gazzano, O.; de Vasconcellos, S. M.; Arnold, C.; Nowak, A.; Galopin, E.; Sagnes, I.; Lanco, L.; Lamaître, A.; Snellart, P. Bright solid-state sources of indistinguishable single photons. *Nat. Commun.* **2013**, *4*, No. 1425.

(7) Kolatschek, S.; Hepp, S.; Sartison, M.; Jetter, M.; Michler, P.; Portalupi, S. L. Deterministic fabrication of circular Bragg gratings coupled to single quantum emitters via the combination of in-situ optical lithography and electron-beam lithography. *J. Appl. Phys.* **2019**, *125*, No. 045701.

(8) Sapienza, L.; Davanço, M.; Lettner, B.; Srinivasan, K. Nanoscale optical positioning of single quantum dots for bright and pure single-photon emission. *Nat. Commun.* **2015**, *6*, No. 7833.

(9) Somaschi, N.; Giesz, V.; De Santis, L.; Loredo, J. C.; Almeida, M. P.; Hornecker, G.; Portalupi, S. L.; Grange, T.; Antón, C.; Demory, J.; Gómez, C.; Sagnes, I.; Lanzillotti-Kimura, N. D.; Lemaître, A.; Auffeves, A.; White, A. G.; Lanco, L.; Senellart, P. Near-optimal single-photon sources in the solid state. *Nat. Photonics* **2016**, *10*, 340−345.

(10) Gyger, S.; Zeuner, K. D.; Lettner, T.; Bensoussan, S.; Carlnäs, M.; Ekemar, L.; Schweickert, L.; Hedlund, C. R.; Hammar, M.; Nilsson, T.; Almlöf, J.; Steinhauer, S.; Llosera, G. V.; Zwiller, V. Metropolitan single-photon distribution at 1550nm for random number generation. *Appl. Phys. Lett.* **2022**, *121*, No. 194003.

(11) Benyoucef, M.; Yacob, M.; Reithmaier, J. P.; Kettler, J.; Michler, P. Telecom-wavelength (1.5μm) single-photon emission from InP-based quantum dots. *Appl. Phys. Lett.* **2013**, *103*, No. 162101.

(12) Holewa, P.; Kadkhodazadeh, S.; Gawełczyk, M.; Baluta, P.; Musiał, A.; Dubrovskii, V. G.; Syperek, M.; Semenova, E. Droplet epitaxy symmetric InAs/InP quantum dots for quantum emission in the third telecom window: morphology, optical and electronic properties. *Nanophotonics* **2022**, *11*, 1515−1526.

(13) Müller, T.; Skiba-Szymanska, J.; Krysa, A.; Huwer, J.; Felle, M.; Anderson, M.; Stevenson, R. M.; Heffernan, J.; Ritchie, D. A.; Shields, A. J. A quantum light-emitting diode for the standard telecom window around 1550nm. *Nat. Commun.* **2018**, *9*, No. 862.

(14) Paul, M.; Olbrich, F.; Höschele, J.; Schreier, S.; Kettler, J.; Portalupi, S. L.; Jetter, M.; Michler, P. Single-photon emission at 1.55 μm from MOVPE-grown InAs quantum dots on InGaAs/GaAs metamorphic buffers. *Appl. Phys. Lett.* **2017**, *111*, No. 033102.

(15) Wroński, P. A.; Wyborski, P.; Musiał, A.; Podemski, P.; Sęk, G.; Höfling, S.; Jabeen, F. Metamorphic Buffer Layer Platform for 1550 nm Single-Photon Sources Grown by MBE on (100) GaAs Substrate. *Materials* **2021**, *14*, No. 5221.

(16) Wyborski, P.; Gawełczyk, M.; Podemski, P.; Wroński, P. A.; Pawlyta, M.; Gorantla, S.; Jabeen, F.; Höfling, S.; Sęk, G. Impact of MBE-grown (In, Ga)As/GaAs metamorphic buffers on excitonic and optical properties of single quantum dots with single-photon emission tuned to the telecom range. *Phys. Rev. Appl.* **2023**, *20*, No. 044009.

(17) Holewa, P.; Vajner, D. A.; Zięba-Ostój, E.; Wasiluk, M.; Gaál, B.; Sakanas, A.; Burakowski, M.; Mrowiński, P.; Krajnik, B.; Xiong, M.; Yvind, K.; Gregersen, N.; Musiał, A.; Huck, A.; Heindel, T.; Syperek, M.; Semenova, E. High-throughput quantum photonic devices emitting indistinguishable photons in the telecom C-band. *Nat. Commun.* **2024**, *15*, No. 3358.

(18) Phillips, C. L.; Brash, A. J.; Godsland, M.; Martin, N. J.; Foster, A.; Tomlinson, A.; Dost, R.; Babazadeh, N.; Sala, E. M.; Wilson, L.; Heffernan, J.; Skolnick, M. S.; Fox, A. M. Purcell-enhanced single photons at telecom wavelengths from a quantum dot in a photonic crystal cavity. *Sci. Rep* **2024**, *14*, No. 4450.

(19) Jeon, W. B.; Moon, J. S.; Kim, K.-Y.; Ko, Y.-H.; Richardson, C. J. K.; Waks, E.; Kim, J.-H. Plug-and-Play Single-Photon Devices with Efficient Fiber-Quantum Dot Interface. *Adv. Quantum Technol.* **2022**, *5*, No. 2200022.

(20) Kaupp, J.; Reum, Y.; Kohr, F.; Michl, J.; Buchinger, Q.; Wolf, A.; Peniakov, G.; Huber-Loyola, T.; Pfenning, A.; Höfling, S. Purcell-Enhanced Single-Photon Emission in the Telecom C-Band. *Adv. Quantum Technol.* **2023**, *6*, No. 2300242.

(21) Sittig, R.; Nawrath, C.; Kolatschek, S.; Bauer, S.; Schaber, R.; Huang, J.; Vijayan, P.; Pruy, P.; Portalupi, S.; M, J.; Michler, P. Thin-film InGaAs metamorphic buffer for telecom C-band InAs quantum dots and optical resonators on GaAs platform. *Nanophotonics* **2022**, *11*, 1109−1116.

(22) Nawrath, C.; Joos, R.; Kolatschek, S.; Bauer, S.; Pruy, P.; Hornung, F.; Fischer, J.; Huang, J.; Vijayan, P.; Sittig, R.; Jetter, M.; Portalupi, S. L.; Michler, P. Bright Source of Purcell-Enhanced, Triggered, Single Photons in the Telecom C-Band. *Adv. Quantum Technol.* **2023**, *6*, No. 2300111.

(23) Kwoen, J.; Imoto, T.; Arakawa, Y. InAs/InGaAs Quantum Dot Lasers on Multi-Functional Metamorphic Buffer Layers. *Opt. Express* **2021**, *29*, 29378−29386.

(24) Kwoen, J.; Zhan, W.; Arakawa, Y. E-band InAs quantum dot laser on InGaAs metamorphic buffer layer with filter layer. *Electron. Lett.* **2021**, *57*, 567−568.

(25) Semenova, E. S.; Kulkova, I. V.; Kadkhodazadeh, S.; Schubert, M.; Yvind, K. Metal organic vapor-phase epitaxy of InAs/InGaAsP quantum dots for laser applications at 1.5μm. *Appl. Phys. Lett.* **2011**, *99*, No. 101106.

(26) Liang, W.; Wei, W.; Han, D.; Ming, M.; Zhang, J.; Wang, Z.; Zhang, X.; Wang, T.; Zhang, J. E-Band InAs Quantum Dot Micro-Disk Laser with Metamorphic InGaAs Layers Grown on GaAs/Si (001) Substrate. *Materials* **2024**, *17*, No. 1916.

(27) Semenova, E. S.; Hostein, R.; Patriarche, G.; Mauguin, O.; Largeau, L.; Robert-Philip, I.; Beveratos, A.; Lemaître, A. Metamorphic approach to single quantum dot emission at 1.55μm on GaAs substrate. *J. Appl. Phys.* **2008**, *103*, No. 103533.

(28) Mansoori, A.; Addamane, S. J.; Renteria, E. J.; Shima, D. M.; Behzadirad, M.; Vadiee, E.; Honsberg, C.; Balakrishnan, G. Reducing threading dislocation density in GaSb photovoltaic devices on GaAs by using AlSb dislocation filtering layers. *Sol. Energy Mater. Sol. Cells* **2018**, *185*, 21−27.

(29) Gourley, P. L.; Drummond, T. J.; Doyle, B. L. Dislocation filtering in semiconductor superlattices with lattice-matched and lattice-mismatched layer materials. *Appl. Phys. Lett.* **1986**, *49*, 1101−1103.

(30) Scaparra, B.; Ajay, A.; Avdienko, P. S.; Xue, Y.; Riedl, H.; Kohl, P.; Jonas, B.; Costa, B.; Sirotti, E.; Schmiedeke, P.; Villafañe, V.; Sharp, I. D.; Zallo, E.; Koblmüller, G.; Finley, J. J.; Müller, K. Structural properties of graded InxGa1-xAs metamorphic buffer layers for quantum dots emitting in the telecom bands. *Mater. Quantum Technol.* **2023**, *3*, No. 035004.

(31) Tersoff, J. Dislocations and strain relief in compositionally graded layers. *Appl. Phys. Lett.* **1993**, *62*, 693−695.

(32) Dunstan, D. J.; Kidd, P.; Howard, L. K.; Dixon, R. H. Plastic relaxation of InGaAs grown on GaAs. *Appl. Phys. Lett.* **1991**, *59*, 3390−3392.

(33) Olsen, J. A.; Hu, E. L.; Lee, S. R.; Fritz, I. J.; Howard, A. J.; Hammons, B. E.; Tsao, J. Y. X-ray reciprocal-space mapping of strain relaxation and tilting in linearly graded InAlAs buffers. *J. Appl. Phys.* **1996**, *79*, 3578−3584.

(34) Sacedón, A.; González-Sanz, F.; Calleja, E.; Muñoz, E.; Molina, S. I.; Pacheco, F. J.; Araújo, D.; García, R.; Lourenço, M.; Yang, Z.; Kidd, P.; Dunstan, D. Design of InGaAs linear graded buffer structures. *Appl. Phys. Lett.* **1995**, *66*, 3334−3336.

(35) Sorokin, S. V.; Klimko, G. V.; Sedova, I. V.; Sitnikova, A. A.; Kirilenko, D. A.; Baidakova, M. V.; Yagovkina, M. A.; Komissarova, T. A.; Belyaev, K. G.; Ivanov, S. V. Peculiarities of strain relaxation in linearly graded In$_x$Ga$_{1−x}$As/GaAs(001) metamorphic buffer layers grown by molecular beam epitaxy. *J. Cryst. Growth* **2016**, *455*, 83−89.

(36) Tomasulo, S.; Simon, J.; Simmonds, P. J.; Biagiotti, J.; Lee, M. L. Molecular beam epitaxy of metamorphic In$_y$Ga$_{1−y}$P solar cells on mixed anion GaAs$_x$P$_{1−x}$/GaAs graded buffers. *J. Vac. Sci. Technol., B: Nanotechnol. Microelectron.: Mater., Process., Meas., Phenom.* **2011**, *29*, No. 03C118.

(37) Jackson, W. B.; Amer, N. M.; Boccara, A. C.; Fournier, D. Photothermal deflection spectroscopy and detection. *Appl. Opt.* **1981**, *20*, 1333−1344.

(38) Dolgonos, A.; Mason, T. O.; Poeppelmeier, K. R. Direct optical band gap measurement in polycrystalline semiconductors: A critical look at the Tauc method. *J. Solid State Chem.* **2016**, *240*, 43−48.

(39) Varshni, Y. Temperature dependence of the energy gap in semiconductors. *Physica* **1967**, *34*, 149−154.

(40) Vurgaftman, I.; Meyer, J. R.; Ram-Mohan, L. R. Band parameters for III−V compound semiconductors and their alloys. *J. Appl. Phys.* **2001**, *89*, 5815−5875.

(41) Syperek, M.; Baranowski, M.; Sęk, G.; Misiewicz, J.; Löffler, A.; Höfling, S.; Reitzenstein, S.; Kamp, M.; Forchel, A. Impact of wetting-layer density of states on the carrier relaxation process in low indium content self-assembled (In,Ga)As/GaAs quantum dots. *Phys. Rev. B* **2013**, *87*, No. 125305.

(42) Wyborski, P.; Podemski, P.; Wroński, P. A.; Jabeen, F.; Höfling, S.; Sęk, G. Electronic and Optical Properties of InAs QDs Grown by MBE on InGaAs Metamorphic Buffer. *Materials* **2022**, *15*, No. 1071.

(43) Cordier, Y.; Chauveau, J.-M.; Ferre, D.; Dipersio, J. Comparison of In$_{0.33}$Al$_{0.67}$As/In$_{0.34}$Ga$_{0.66}$As on GaAs metamorphic high electron mobility transistors grown by molecular beam epitaxy with normal and inverse step on linear graded buffer layers. *J. Vac. Sci. Technol., B: Microelectron. Nanometer Struct.–Process., Meas., Phenom.* **2000**, *18*, 2513−2517.

(44) Cordier, Y.; Lorenzini, P.; Chauveau, J.-M.; Ferré, D.; Androussi, Y.; DiPersio, J.; Vignaud, D.; Codron, J.-L. Influence of MBE growth conditions on the quality of InAlAs/InGaAs metamorphic HEMTs on GaAs. *J. Cryst. Growth* **2003**, *251*, 822−826. Proceedings of the Twelfth International Conference on Molecular Beam Epitaxy.

(45) Romanato, F.; Napolitani, E.; Carnera, A.; Drigo, A. V.; Lazzarini, L.; Salviati, G.; Ferrari, C.; Bosacchi, A.; Franchi, S. Strain relaxation in graded composition In$_x$Ga$_{1−x}$As/GaAs buffer layers. *J. Appl. Phys.* **1999**, *86*, 4748−4755.

(46) Jung, D.; Norman, J.; Kennedy, M. J.; Shang, C.; Shin, B.; Wan, Y.; Gossard, A. C.; Bowers, J. E. High efficiency low threshold current 1.3μm InAs quantum dot lasers on on-axis (001) GaP/Si. *Appl. Phys. Lett.* **2017**, *111*, No. 122107.

(47) Häusler, K.; Eberl, K.; Noll, F.; Trampert, A. Strong alignment of self-assembling InP quantum dots. *Phys. Rev. B* **1996**, *54*, 4913−4918.

(48) Abbarchi, M.; Mastrandrea, C.; Kuroda, T.; Mano, T.; Vinattieri, A.; Sakoda, K.; Gurioli, M. Poissonian statistics of excitonic complexes in quantum dots. *J. Appl. Phys.* **2009**, *106*, No. 053504.

(49) Young, R. J.; Stevenson, R. M.; Shields, A. J.; Atkinson, P.; Cooper, K.; Ritchie, D. A.; Groom, K. M.; Tartakovskii, A. I.; Skolnick, M. S. Inversion of exciton level splitting in quantum dots. *Phys. Rev. B* **2005**, *72*, No. 113305.

(50) Langbein, W.; Borri, P.; Woggon, U.; Stavarache, V.; Reuter, D.; Wieck, A. D. Control of fine-structure splitting and biexciton binding in $In_xGa_{1-x}As$ quantum dots by annealing. *Phys. Rev. B* **2004**, *69*, No. 161301.

(51) Sapienza, L.; Malein, R. N. E.; Kuklewicz, C. E.; Kremer, P. E.; Srinivasan, K.; Griffiths, A.; Clarke, E.; Gong, M.; Warburton, R. J.; Gerardot, B. D. Exciton fine-structure splitting of telecom-wavelength single quantum dots: Statistics and external strain tuning. *Phys. Rev. B* **2013**, *88*, No. 155330.

(52) Skiba-Szymanska, J.; Stevenson, R. M.; Varnava, C.; Felle, M.; Huwer, J.; Müller, T.; Bennett, A. J.; Lee, J. P.; Farrer, I.; Krysa, A. B.; Spencer, P.; Goff, L. E.; Ritchie, D. A.; Heffernan, J.; Shields, A. J. Universal Growth Scheme for Quantum Dots with Low Fine-Structure Splitting at Various Emission Wavelengths. *Phys. Rev. Appl.* **2017**, *8*, No. 014013.